FERMILAB-PUB-11-687-T

Associated production of W/Z gauge bosons and jets in hadronic collisions

John Campbell

Fermilab, Theory Group, Batavia, IL 60510, USA

Michelangelo Mangano

CERN, TH-PH, 1211 Geneva 23, Switzerland

Key Words Hadron Collisions; Tevatron; LHC; QCD; Vector bosons

Abstract Most new particles predicted by theories beyond the Standard Model of particle physics decay to jets and electroweak gauge bosons, W and Z. The search and study of these particles requires therefore a solid understanding of the associated production of W/Z and jets. This review provides an introduction to the theoretical and experimental aspects of these processes in the context of the Standard Model. First we introduce the challenges presented by the calculation of the production properties of W/Z plus jets in hadronic collisions, and review the tools developed to characterize quantitatively such final states. Then we summarize the current experimental results, at the Tevatron and LHC colliders, and discuss the comparison between the available data and the theoretical predictions.

CONTENTS

INTRODUCTION 2

Operated by Fermi Research Alliance, LLC under Contract No. DE-AC02-07CH11359 with the United States Department of Energy

THEORETICAL TOOLS 4

Fixed-order, parton-level calculations 6

Shower MC description of final states 10

COMPARISONS BETWEEN THEORY AND EXPERIMENTAL DATA 13

General aspects of the experimental measurements 14

Tevatron results on V plus light jets 18

Tevatron: associated production with heavy quarks 20

LHC: first findings 24

CONCLUSIONS AND OUTLOOK 26

1 INTRODUCTION

The main goal of today's high-energy colliders is the search for new particles that could shed light on some of the key puzzles of the Standard Model (SM) description of fundamental interactions: what is the origin of electroweak symmetry breaking? What is the origin of dark matter? Are there additional interactions, symmetries, or new layers of structure beyond the SM? All models introduced to address these questions predict the existence of new particles, and in most cases these particles are heavier than all the known ones, typically in the 100 GeV to a few TeV range. Aside from few exceptions, these new particles are either neutral, weakly interacting and stable, or sequentially decay to leptons, quarks and possibly gluons and photons. In the former case, the experimental signature amounts to an apparent violation of energy conservation, as in the case of the emission of a neutrino, which carries away energy undetected (a "missing energy" signature). In the latter case, due to the large mass of the parents, the decay products have high energy and, in the case of quarks and gluons, manifest themselves as jets,

namely collimated streams of hadrons.

The generic signature of production and decay of new particles includes, therefore, a mixture of leptons and jets (1). Leptons and jets, on the other hand, can also arise from SM processes, such as the associated production of gauge bosons (W and Z), quarks and gluons, where the decay of the gauge bosons can lead to the desired lepton signatures. For example, the associated production with a W boson can lead to final states with a charged lepton, missing energy and jets, while associated production with a Z boson decaying to a $\nu\bar{\nu}$ pair would lead to final states with jets and missing energy.

Associated production of gauge bosons and jets is not only a background to possible physics beyond the SM (BSM), but is an important background to the search and study of SM particles like the top quark, or the elusive Higgs boson. The reason is that, once again, the heavy top quark and Higgs boson sequentially decay down to the lightest states in the spectrum, namely leptons and quarks lighter than the top. The study of V+jets production (V=W or Z) is therefore a necessary tool both to search for new objects, and to carry out more accurate studies of the still-poorly known top quark.

In this review we outline the status of the theoretical understanding of V+jets production at hadronic colliders, showing how the predictions compare against the measurements at the Tevatron and at the LHC.

Section 2 will introduce the available theoretical tools: *(i)* calculations at a fixed-order in perturbation theory; *(ii)* calculations based on the merging of leading-order (LO), parton-level predictions, with a description of higher-order radiative processes, leading to the full-fledged development of quarks and gluons into jets, and to their subsequent transformation into physically-observable

hadrons.

Section 3 will summarize the available data, both from the Tevatron and from the LHC, and assess the level of agreement between predictions and observations. The conclusions in Section 4 will discuss the directions for future theoretical improvement, and the opportunities offered by new forthcoming measurements to further improve the understanding of this class of processes.

2 THEORETICAL TOOLS

The theoretical description of V+jets production cross sections, and of the properties of the final states, rely on perturbative quantum chromodynamics (QCD). This is possible since the mass of the gauge bosons, and the transverse energy E_T of the jets, are both much larger than the scale $\Lambda \sim 1$ GeV at which the interactions among partons (i.e. quarks and gluons) become non-perturbative. This makes it possible to factorize the calculations into three steps (for recent reviews, see e.g. (2,3)): (*i*) the evaluation of the matrix elements for the elementary parton-level scattering process, in which quarks and gluons inside the two colliding hadrons interact to produce V and a number of energetic partons; (*ii*) the convolution of the corresponding parton-level cross section with the densities of quarks and gluons inside the colliding hadrons (parton distribution functions, PDFs); (*iii*) the modeling of the evolution of the final-state partons into hadrons and full-fledged jets.

The evolution of partons into jets conserves momentum and flavor. Therefore, although jets are made of varying numbers and types of particles, it is possible, with appropriate jet definitions (5), to identify their inclusive properties (e.g. the momentum) with those of the partons that originate them. The first two steps

outlined above are therefore sufficient to give quantitative predictions for inclusive observables such as the energy distributions and angular correlations of jets. The precision of these predictions is driven by the accuracy of the perturbative calculation of the matrix elements and of the determination of the PDFs. The first part of this Section will review the status of these calculations.

The experimental analyses of these final states, nevertheless, require a more detailed description of their features. For example, particles produced by the interaction of fragments of the beam hadrons could point in the same direction as jets produced in the primary collisions, and contribute to the jets' energies. Likewise, hadronization, namely the process that turns quarks and gluons into physical particles, will force some amounts of energy to be lost or acquired by jets. This is because the individual quark or gluon that originates the jet is colored, while the physical jet itself is made of color-less particles. The neutralization of color arises from the exchange of at least one colored parton among jets, a process which is modeled in the third step outlined above. The QCD perturbative evolution of partons, via multiple emissions of gluons and quarks, and the phenomenological modeling of their hadronization and of the collision among the beam fragments, are evaluated via the so-called shower Monte Carlo (MC) event generators (for an elementary introduction see (3), while an extended review of the latest progress is documented in (6)). Several of these numerical codes have become standard tools, used for both theoretical and experimental studies: PYTHIA (7,8), HERWIG (9,10) and SHERPA (11). The second part of this section will review the specific issues raised by the merging of multiparton final states with the shower MC codes, and describe the tools that have been recently developed to address them.

2.1 Fixed-order, parton-level calculations

Comprehensive studies of V+jet final states in fixed order began with the advent of LO MC predictions for $W + 4$ jet and $Z + 3$ jet final states (12). Predictions at the next-to-leading order (NLO) began with studies of vector bosons recoiling against a single jet (13–16) and were much later extended to the case of $V + 2$ jets (17,18). Most recently, new techniques for calculating loop corrections numerically have led to NLO predictions for $W + 3$ jet (19–22), $Z + 3$ jet (23) and $W + 4$ jet (24) production. Calculations of the production of vector bosons with heavy quarks, which are more challenging than when considering massless partons, are available at NLO for the cases of heavy quarks produced both singly (25–27) and in pairs (28–31). We note in passing that recent progress in the calculation of higher order corrections, in particular new automatic calculations of multiparton NLO cross sections (32), will likely result in further results for related processes in the near future.

The main drive to include NLO corrections to these processes is in order to provide a more accurate description of them, not only in terms of the total rate of such events but also when considering kinematic quantities such as the jet transverse momenta. In the most broad sense the quality of the prediction is clearly improved by including more terms in the perturbative expansion. The inclusion of real radiation diagrams that include an additional parton allows some sensitivity to the structure of the jets in the final state. At the same time such NLO diagrams can also contain new parton species in the initial state, an issue of particular relevance at the LHC where the gluon PDF dominates over the quark one. However, these qualitative reasons that improvement should be expected are usually overshadowed by the more quantitative measure of scale dependence.

At a finite order of the perturbative expansion any physical prediction contains dependence on the renormalization and factorization scales used in the definitions of the strong coupling and PDFs respectively. Although the typical factorization scale dependence of a LO prediction is weak, the renormalization scale dependence is much bigger and simply scales with the number of jets. For this reason the LO predictions can be considered estimates only. At NLO this scale dependence is *formally* improved, with terms in the NLO calculation explicitly canceling the LO scale dependence. The residual dependence remaining is suppressed by a factor of the strong coupling, but can of course still be large in practice. Nevertheless the canonical situation is that the scale dependence observed at NLO is much reduced compared to that seen at LO.

A common procedure for estimating the theoretical uncertainty on a prediction is to choose a central scale and then vary the scale by a factor of two in each direction about this choice. As an example, the uncertainties resulting from using such a procedure for W^-+ jet production at the 7 TeV LHC is shown in Figure 1 (adapted from results presented in Ref. (24)). In these predictions, the central scale choice is given by $\hat{H}_T/2$, where $\hat{H}_T$ is the sum of the (scalar) transverse momenta of the W decay products and partons. It is clear that the estimated uncertainty on the LO prediction grows with the number of jets but is substantially reduced at NLO. Any procedure for estimating the theoretical uncertainty by varying the scale in this way may be viewed as somewhat arbitrary, with the choice of a factor of two representing perhaps only a bare minimum. In addition one might also choose to separately vary the factorization and renormalization scales in case of accidental cancellation between the two. It is certainly not guaranteed that the envelope of scale uncertainty at any given order in perturbation

theory will overlap with the prediction from the next order higher. An example of such a situation can be seen in the $W+1$ jet prediction in Figure 1, where the difference is understood to be related to the large gluon-gluon flux that can contribute only beyond LO.

Furthermore, the question of which central scale to choose when evaluating the fixed-order (LO or NLO) prediction does not have an unambiguous answer. For inclusive V production the only physical scale present in the process is the gauge boson mass (M_V), a natural choice. In the presence of an additional jet each event has a further characteristic scale, namely the transverse momentum of the jet ($p_T^{\rm jet}$). At LO this is equivalent to the transverse momentum of V (p_T^V), although even this simple relation is broken at NLO. So, even for the simplest case of V+jet, one could argue that any combination of M_V, p_T^V and $p_T^{\rm jet}$ might be appropriate. In the presence of further jets this picture is of course complicated still further, an issue that has been particularly brought into focus by the latest $V+3,4$ jet NLO predictions.

As an illustration of this issue, consider the transverse energy spectrum of the second leading jet in W^-+3 jet events. Predictions from LO and NLO calculations are shown in Figure 2 for two different event-by-event scale choices. The two scales used are the transverse energy of the W boson ($E_T^W = \sqrt{M_W^2 + (p_T^W)^2}$) and $\hat{H}_T$. While the choice $\mu = \hat{H}_T$ yields very small corrections, choosing $\mu = E_T^W$ generates substantial NLO corrections that result in unphysical (negative) event rates at sufficiently large jet E_T. An explanation of the more satisfactory description of the $\hat{H}_T$ scale is that the dominant kinematic configurations at moderate to high E_T are ones in which two hard jets are almost balanced, with further jets and the vector boson relatively soft. In that case scales related to the momentum

of the vector boson would not be expected to perform well (20). Nevertheless, while it is clear that the choice $\mu = E_T^W$ is not suitable in this case, the large NLO corrections identified using this scale highlight the complexity of the logarithmic structure of NLO contributions in general. In particular, they underscore the difficulty in identifying a functional form for the renormalization scale that can serve as a reliable reference throughout the full phase-space. For example while the scale $\mu = \hat{H}_T$ is apparently adequate to describe inclusive jet E_T spectra, it may fail to properly characterize large logarithms appearing in very asymmetric kinematical configurations, where several scales are present. For example, configurations where a few jets have energies much larger than M_V, and others much smaller than M_V, or where the various dijet pairs in the final state have invariant masses M_{jj} distributed over a very broad range, $M_{jj}^{\rm min} \ll M_V \ll M_{jj}^{\rm max}$. We consider the reliable determination of the NLO scale uncertainty for these multi-parton final states to be still an open issue. Its understanding will require further theoretical work, and will greatly benefit from experimental measurements of a wider variety of multijet observables, in particular at the LHC, where the higher energy allows access to a much larger kinematic range.

A large uncertainty that must be accounted for when comparing with experimental data is that coming from non-perturbative effects. Such corrections are usually estimated by comparison of data with shower MCs and can be much larger than the scale uncertainties discussed here. The next subsection will review this topic, in the context of LO calculations. The systematic assessment of such effects in the presence of NLO cannot be explored until NLO shower MCs are available for these processes. The first steps towards this, in the form of a NLO shower MC for $V + 1$ jet production, are just now being taken (33).

2.2 Shower MC description of final states

The relation between parton-level jets generated in a theoretical calculation, and the real jets reconstructed by a detector, is not clear cut. On one side, instrumental effects can alter the structure of individual jets, affecting the jet counting. For example, the real measurement of a jet energy can fluctuate low, and an n-jet event appears as having $(n-1)$ jets only. Likewise, a small dead region in the detector acceptance could split a single broad jet into two separated jets, increasing the jet multiplicity by 1. There are also theoretical reasons that require the merging of events generated with different parton multiplicities. The addition of the shower evolution to a fixed-order partonic final state may in fact lead to a number of reconstructed jets that can both be smaller or larger than the number of original final-state partons. The former case can happen via multiple large-angle soft emission, smearing the parton energy over a volume bigger than the jet size. The latter can occur via one or more hard emissions at large angle, from both the initial and the final-state partons. We are therefore unavoidably led to the need to merge together calculations (and simulated event samples) corresponding to different jet multiplicities.

To achieve this, the calculations need to describe as accurately as possible both the full matrix elements for the underlying hard processes, as well as the subsequent development of the hard partons into jets of hadrons. However, for the complex final-state topologies we are interested in, no factorization theorem exists to rigorously separate these two components. The main obstacle is the existence of several hard scales, like the jet transverse energies and dijet invariant masses, which for a generic multijet event will span a wide range. This makes it difficult to unambiguously separate the components of the event belonging to the hard

process (to be calculated using a multiparton scattering amplitude) from those arising during its evolution (described by the parton shower). A given $(n+1)$-jet event can be obtained in two ways: from the collinear/soft-radiation evolution of an appropriate $(n+1)$-parton final state, or from an n-parton configuration where hard, large-angle emission during its evolution leads to the extra jet. A factorization prescription (in this context this is often called a 'matching scheme' or 'merging scheme') defines, on an event-by-event basis, which of the two paths should be followed. The primary goal of a merging scheme is therefore to avoid double counting (by preventing some events from appearing twice, once for each path), as well as dead regions (by ensuring that each configuration is generated by at least one of the allowed paths). Furthermore, a good merging scheme will optimize the choice of the path, using the one which guarantees the best possible approximation to a given kinematics. It is possible to consider different merging schemes, all avoiding the double counting and dead regions, but leading to slightly different results in view of the different ways the calculation is distributed between the matrix element and the shower evolution. As in any factorization scheme, the physics is independent of the separation between phases only if we have complete control over the perturbative expansion. Otherwise a residual scheme-dependence is left. Exploring different merging schemes is therefore crucial to assess the systematic uncertainties of multijet calculations.

Three matching algorithms have been developed and are used in phenomenological applications: the CKKW scheme (34,35), the Lönnblad scheme (36) and the MLM scheme (37). These merging procedures follow a similar strategy. To start with, parton-level events with different partonic multiplicity $n = 0, 1, \ldots, N_{max}$ are independently generated to cover the full $V + n$ partons phase space. They

are selected with a probability proportional to the perturbative matrix elements squared, weighted by the phase-space density. When one of these parton-level events, with $n = n_0$, is later evolved through a shower MC, additional n_j jets may arise due to hard radiation, leading to a potential double counting with events from the sample that had $n = n_0 + n_j$ hard partons to start with. It is known that the approximations built into the shower MC are inadequate to describe hard large-angle radiation, and the merging schemes therefore aim at ensuring that an event with n final-state jets arises only from the evolution of a parton-level event with precisely n final-state partons. The removal of the extra events is enforced in either of two ways. One can reweight the cross-section of a parton-level event, multiplying by a so-called Sudakov form factor, which measures the probability that a given parton does not evolve emitting radiation leading to secondary jets. Any such emission will then be vetoed during the evolution through the shower MC. This is the technique used in the CKKW scheme. Or, as is qualitatively done in the other two schemes, one can simply allow the event to evolve through the shower MC, and reject events where extra jets were radiated, removing their contribution to the cross section.

An early application of the CKKW scheme to W+jets final states was discussed in (38), while a thorough comparison among the predictions for W+jets of all three schemes, as implemented in five different MC generators (11, 39–42), is documented in (43).

Examples of these comparisons, for jet E_T spectra at the Tevatron and at the LHC ($\sqrt{S}$ = 14 TeV), are shown in Figs. 3 and 4, taken from Ref. (43). One can notice that, with one exception, all calculations agree to within ±30% both in absolute rates and in shapes. This spread is consistent with the systematic

uncertainty of each individual prediction, due to their LO character. It is important to notice that the quality of the agreement among different calculations is preserved at the higher energy of the LHC.

Additional phenomenological studies of W+jets final states are documented in Refs. (44, 45). In the following section we shall illustrate how these results compare against the actual data, from both the Tevatron and the LHC.

Future progress will come from the extension of merging procedures to samples generated using NLO partonic calculations. The starting point for these developments is the introduction of a consistent matching between NLO partonic processes and shower MCs. This requires the removal of the double counting between the radiative corrections present in the NLO calculation (both real and virtual emissions) and those generated by the shower evolution. For fixed-multiplicity NLO results this has been achieved in concrete, fully fledged, codes such as MC@NLO (46,47) and POWHEG (48,49). Work is in progress to improve these approaches with higher-multiplicity, LO matrix-element corrections (50,51).

3 COMPARISONS BETWEEN THEORY AND EXPERIMENTAL DATA

We begin the review of the comparison between theory and data with an introduction to some key aspects of the experimental analyses. We address the definition of observables suitable for a comparison with theory, the interplay of theoretical and experimental systematics, and the sources of backgrounds. After this, we present a survey of the current published results from the Tevatron and the LHC. We focus our discussion on V+multijet final states; measurements of inclusive properties of W/Z production (total cross section, p_T spectra) are

documented in Refs. (52–55) for the Tevatron, and in (56, 57) for the LHC.

3.1 General aspects of the experimental measurements

A large number of studies of the properties of V+jets final states have been performed by the Tevatron collaborations, and more recently at the LHC, in the context of the measurements of the $t\bar{t}$ and single-top-quark cross sections, in the searches for the Higgs boson, and in the search for several BSM phenomena. The goal of most of these studies is to validate the estimates of the V+jets backgrounds, often using a combination of data (for the normalization of the production rates in background-dominated control regions) and MC simulations (to model the extrapolation to the signal regions). While essential for the experimental purposes, these studies only give limited input for the verification and improvement of the theoretical calculations, since they are based on processing the output of MC event generators through the software modeling the detector response. To directly compare theoretical predictions with data, and in particular to test parton-level NLO calculations, experiments need to correct their data to the so-called hadron level. This means compensating for all detector-related effects, from measurement inefficiencies, to the unsmearing of the jet energies, reporting final cross sections corresponding to the true energies of the physical particles arising from the collision. Due to the complexity of these corrections, only a few of the existing experimental measurements report results corrected to the hadron level.

Hadron-level experimental results can be compared directly with the results of full shower-MC calculations, which describe not only the complete hadronization of the components of the hard process, but also the so-called underlying event

(UE), namely the particles produced by the collision and evolution of the beam fragments. The comparison with parton-level NLO calculations, vice-versa, requires the explicit inclusion of such non-perturbative effects, via the modeling of both hadronization and UE. This is because only a small number of NLO calculations are available in the form of full-fledged shower MC, and they are limited to final states with small jet multiplicity. For a given observable X (e.g. a jet energy), one assumes that the non-perturbative effects affect in the same way the LO and the NLO parton-level cross sections. One thus considers the cross section $d\sigma/dX$ calculated using different components of the MC-generated LO final states: $d\sigma_{PL}/dX$ is calculated using the partons emerging from the shower evolution, switching off both hadronization and the collision between the fragments of the beam particles. $d\sigma_{had}/dX$ is calculated using all hadrons, after the inclusion of both hadronization and the collisions of the beam fragments. The correction factor $C_{had}(X) = [d\sigma_{had}/dX]/[d\sigma_{PL}/dX]$ is then applied to the NLO computation of the X distribution, before comparison with the data.

For $X = E_T$, the effects of hadronization and of the UE have opposite sign: the fragments of the initial-state hadrons will increase the jet energy, and thus the cross section. The hadronization will slightly reduce it. $C_{had}(X)$ can be calculated for any observable quantity X using a shower MC. It can be both larger and smaller than 1, depending on the variable and on the precise jet definition. For energy-like quantities, such as the jet transverse energies, C_{had} approaches 1 as the energy increases, consistently with the non-perturbative origin of the corrections. Different MC models, or different model parameters, are used to assess the systematic uncertainty on C_{had}. Some explicit examples will be given below.

Another important ingredient of the comparisons between data and theory is the choice of whether or not to correct for the incomplete detector acceptance. Typical analyses of vector-boson final states, to ensure an optimal detection efficiency and background rejection, impose on the decay leptons a minimum transverse momentum and a maximum rapidity. In the past it was customary to use a MC calculation to estimate the loss of acceptance due to these cuts, and correct accordingly the measured cross sections. These estimates had to include the uncertainties in the modeling of the extrapolation to the full kinematical range (e.g. due to the choice of PDFs), introducing artificial systematics not of experimental origin, and often hard to deal with in a theoretical interpretation of the results. Since modern calculations, even those at NLO, can be performed in the presence of kinematical cuts, the most recent experimental measurements are reported without acceptance corrections.

W bosons are produced in hadronic collisions approximately three times more often than Z bosons, with a very mild dependence on the beam energy, the beam types, and on the multiplicity of associated jets. This is the consequence of the quark couplings to W and Z bosons, and of the relative fraction of quark flavors inside the proton. The total rates for W (Z) bosons increase from $\sim$25 (8) nb at the Tevatron (52), to $\sim$90 (30) nb for the LHC at $\sqrt{S} = 7$ TeV (56,57). Including the branching fractions for leptonic decays results in ($W \to \ell\nu$)+jets rates $\sim$6 times larger than those of ($Z \to \ell^+\ell^-$)+jets.

Z+jet final states compensate the lower rate with a very clean signature (the dilepton invariant-mass peak, integrated over a typical range $|M(\ell^+\ell^-) - M_Z| \sim 20 - 30$ GeV) and with an accurate reconstruction of the Z boson momentum, through its decay products. W+jet final states are subject to a variety of pos-

sibly large backgrounds. Production and decay of top quark pairs is the leading background for $N_{jet} \geq 4$, particularly at the LHC, where the ratio $\sigma(t\bar{t})/\sigma(W)$ is approximately ten times larger than at the Tevatron. Inclusive QCD jets, in particular those originating from pair-produced charm and bottom quarks, are an important background at smaller N_{jet}. These final states can fake the W signature through the concurrent semileptonic decay of the heavy quarks, one leading to a charged lepton carrying most of the heavy quark energy, the other leading to an energetic neutrino.

One interesting feature of the V+jets cross sections is the approximately constant ratio $R_n = \sigma_{V+n}/\sigma_{V+(n-1)}$, a property known as "Berends scaling". R_n depends on the beam energy, on the kinematical cuts and on the algorithm used to define the jets, but it otherwise appears to be rather constant with n, at least for not too large jet E_T thresholds. This property was first observed in the LO, parton-level calculations of V+multijet rates (12, 58), and was then confirmed by the data. Berends scaling has no fundamental origin, except reflecting the fact that, due to the large mass of the V boson, the further addition of a few extra jets with transverse momenta much smaller than M_V constitute a sequence of small and comparable perturbations to the main dynamics of the underlying V production process. Since producing a W requires 80 GeV of energy, the energy threshold to add, for example, a 10 GeV jet, is only 12% higher, and 11% higher to produce a second jet. This gives an approximately constant relative increase in the values of the initial-state parton momenta x required to generate these higher-order final states, and an approximate scaling in the reduction of the relative parton luminosities. This consideration suggests that, as the jet energy increases, Berends scaling becomes less accurate. This is shown in some exam-

ples, for the Tevatron and LHC, in Tables 1 and 2. For simplicity, we use here the simple LO, parton-level calculation of the cross sections[1], which is known to reproduce the NLO behavior of R_n. Strong deviations from R_n scaling can be seen for jet thresholds above 20 GeV. The largest difference appears between R_1 and R_2, reflecting the fact that adding a high-E_T jet to an individual V has a bigger impact on the rates than adding further jets when some are already present. This effect is enhanced by the fact that adding a single jet to a V demands extra kinetic energy to let the V recoil against the jet, something which is not necessary for $n > 1$. The values of R_n tend to become closer to each other for larger n, but at some point R_n will need to decrease, due to the saturation of the available phase-space. Notice also that R_n is larger at the LHC for a given jet threshold, as expected due to the much greater phase-space available. We conclude that, while Berends scaling can give some approximate estimate of the rates for larger numbers of jets, it cannot be used as a reliable tool to extrapolate V+jet rates.

The data discussed below will provide several examples of both agreement and departure from Berends scaling, consistent with the picture provided above.

3.2 Tevatron results on V plus light jets

The CDF experiment has published the cross sections and transverse energy spectra of final states with a $W \to e\nu$ and $N_j = 1, \ldots, 4$ jets (60), using an integrated luminosity of 320 pb^{-1}. Jets were reconstructed using a cone algorithm with radius 0.4, and required to have $E_T > 25$ GeV and $|\eta| < 2$. The jets' E_T distributions are corrected to the hadron level, and the electrons have

[1]For reference, we used the CTEQ5L PDF parameterization (59), renormalization scale $\mu^2 = M_W^2 + \sum_{jets} E_T^2$, $\Delta R_{jj} > 0.7$ and $|\eta_j| < 2.5$.

$E_T > 20$ GeV and $|\eta| < 1.1$. The comparison with the NLO parton-level results, given for $N_j = 1, 2$ by the MCFM calculation (17, 18), and with two implementations (38, 39) of multijet matrix element plus shower matching calculations, is shown in fig. 5. The NLO prediction, which has, as shown, a rather small systematic uncertainty, is in excellent agreement with the data. Recent calculations of the NLO rate for the 3-jet channel also agree with these data (21, 22). The LO matched calculations, while low by a factor of about 40-50%, describe precisely the ratios R_n, which are shown in the lower inset of fig. 5, and compared there to the theory predictions.

A comparison of the jet E_T shapes with theory is also given in (60), showing again a very good agreement with the NLO results. The dataset on which this analysis is based represents only a small fraction of the full integrated luminosity collected by the Tevatron experiments. Higher statistics studies by both experiments, extending the range in the jets E_T to higher values, and possibly reaching $N_j > 4$, will hopefully appear soon.

The Z+jets cross sections, with up to three jets, have been measured by both CDF (61) and D0 (62, 63). The results for the leading jet are shown in fig. 6, compared to the NLO calculation of (23). Both experiments use a midpoint jet algorithm (64), with a cone size of $R = 0.7$ for CDF and $R = 0.5$ for D0. This difference is reflected in the different size of the non-perturbative corrections embodied in the C_{had} coefficient introduced earlier. The solid lines in the lower insets of the plots in fig. 6 correspond in fact to the ratio of partonic and hadronic NLO rates, thus precisely to $1/C_{had}$. For the bigger CDF cone the correction C_{had} is bigger than 1 (65), and as large as 1.2 for low E_T, reflecting the larger amount of UE energy deposited in the bigger cone. For the D0 cone size, the fragmentation

and UE effects almost cancel each other (63), to within a few percent. In both cases, the agreement of data and theory is nevertheless excellent, well within the experimental and the (smaller) theoretical uncertainties. This remains true for the distributions of the second and third jet, shown in fig. 7.

Further tests of the production dynamics, and comparisons with the predictions of both NLO QCD and matrix elements plus shower MC calculations, have been performed by D0, by studying the angular correlations between the Z boson and the leading jet in Z+jet final states (66). As in the case of the W+jets studies, all analyses using Z bosons, which are subject experimentally to much smaller systematics, and which today represent only between 1 and 2.5 fb^{-1} of data, will benefit from the inclusion of the full available Tevatron datasets.

3.3 Tevatron: associated production with heavy quarks

The subset of V+jets events where some of the jets arise from the evolution of heavy quarks (charm and bottom) is of particular interest, since the presence of such heavy quarks in these final states is a specific signature of the decay of top quarks, and is often also a feature of the decay of new particles, for example Higgs bosons, new quark flavours or scalar supersymmetric partners of the common quarks.

There are two main classes of SM processes with gauge bosons and heavy quarks: production of a single charm quark in association with a W boson, and pair production of $Q\overline{Q}$ pairs ($Q = c, b$). The former is due to the Cabibbo transition of a strange or down quark, which transforms into a charm via emission of the W. The latter typically follows from the splitting of a gluon into a $Q\overline{Q}$ pair, either in the initial, or in the final state. We review these two sets of processes

separately. We note here that the associated production of photons and heavy quarks has also been measured by D0 (67) and by CDF (68), but we shall not review these studies here.

3.3.1 Wc PRODUCTION The leading production channel is the reaction $gs \to Wc$. This is directly proportional to the strange-quark content of the proton, and is therefore a direct probe of the strange-quark PDF (26, 69), whose uncertainty dominates the theoretical systematics in the calculation of the relative cross section, of order $\pm 30\%$. Precise measurements could therefore result in improved constraints on this PDF, an improvement that would reduce the overall uncertainty on the inclusive W and Z production rates, particularly at the LHC (4). Both CDF (70) and D0 (71) have measured this final state, using the semileptonic muon decay of the charm quark and the correlation with the charge of the W boson as identification tags. CDF, using 1.8fb^{-1} of data, measured $\sigma_{Wc}(p_T^c > 20 \text{ GeV}, |\eta_c| < 1.5) \times \text{BR}(W \to \ell\nu) = 9.8 \pm 3.2$ pb, in agreement with the NLO prediction of $11.0^{+1.4}_{-3.0}$ pb (26). D0 measured the ratio $\sigma_{Wc}/\sigma_{W\,jet} = 0.074 \pm 0.019_{\text{stat}}\,{}^{+0.012}_{-0.014}{}_{\text{syst}}$, over 50% higher than a LO prediction of 0.044 ± 0.003. The precision of these measurements is still insufficient to draw significant conclusions, and the analysis of the much larger, available, data samples, including the measurement of the charm-jet energy spectrum, will be necessary for more compelling tests.

3.3.2 $VQ\overline{Q}$ PRODUCTION Associated production of gauge bosons and $Q\overline{Q}$ pairs can itself be separated into two sets, depending on whether one or two jets containing any heavy quark are reconstructed. The latter case trivially arises when Q and $\overline{Q}$ are produced at sufficiently large E_T and well separated from each other. The former case can arise under several circumstances: the $Q\overline{Q}$ pair

can be very close, and thus both Q and $\overline{Q}$ fall within the same jet; one of the quarks is too soft to reconstruct a jet; or, finally, one of the two quarks is produced at very large rapidity and is outside the detector acceptance. Contrary to the case of light quarks, where each of these last circumstances would lead to an infrared or collinear divergence in the cross section, the heavy quark mass ensures its finiteness. The reason for this is that the quark mass guarantees that final states with even an infinitely soft quark, or an exactly collinear $Q\overline{Q}$ pair, are physically observable (e.g. through their decays). The heavy quark mass, on the other hand, introduces a new energy scale in the problem, in addition to M_V and to the jet E_T. As a result, there is a potential for the appearance, in the theoretical cross sections, of new large logarithms and of large radiative corrections, which may need to be resummed in order to achieve reliable predictions. This is not the case for final states with two identified heavy-quark jets, since in this case the dynamics is controlled by the jet energy, rather than by the quark mass. On the other hand, these logarithms appear in the case of final states with only one heavy-quark jet. For example, integrating one of the quarks at small E_T and large rapidity will lead to $\log(M_W/M_Q)$ terms, while integrating over the phase-space defining a jet containing both Q and $\overline{Q}$ leads to $\log(E_T^{jet}/M_Q)$ terms.

The above considerations make the measurement of associated $VQ\overline{Q}$ production very interesting. CDF has measured the cross section for production of inclusive production of a b-quark jet and W bosons (72), using 1.9fb^{-1} of data. The W is defined by the presence of a lepton (e or μ) with $p_T > 20$ GeV and $|\eta_\ell| < 1.1$, plus missing energy corresponding to a neutrino $p_T > 25$ GeV. The b-jet satisfies $|\eta_{b-jet}| < 2$ and $E_T^{b-jet} > 20$ GeV. The resulting cross-section, including the semileptonic branching ratio, is $2.47 \pm 0.27_{\rm stat} \pm 0.42_{\rm syst}$ pb, twice

as large as the NLO prediction of Ref. (27) of 1.22 ± 0.14 pb. An even larger discrepancy, of order 3, is observed in the comparison with LO matrix-element plus shower MC calculations, like ALPGEN (39).

The $Z + b$-jet process has been studied by both CDF (73) and D0 (74). CDF, using 2fb^{-1} of data, measures the fraction of inclusive Z events containing a b jet with $E_T^{b-jet} > 20$ GeV and $|\eta_{b-jet}| < 1.5$, finding $3.32 \pm 0.53_{\rm stat} \pm 0.42_{\rm syst} \times 10^{-3}$. This also corresponds to a fraction of the inclusive Z+jet events of $2.08 \pm 0.33_{\rm stat} \pm 0.34_{\rm syst} \times 10^{-2}$. NLO QCD, as quoted in (73), predicts $2.5 \pm 0.3 \times 10^{-3}$ for the former measurement, and $2.0 \pm 0.2 \times 10^{-2}$ for the latter one. Both these results, and the predictions obtained from LO shower MC tools (73), are in reasonable agreement with the data.

D0, using 0.18fb^{-1} of data (74), measures the fraction of inclusive Z+jet events containing a b jet with $E_T^{b-jet} > 20$ GeV and $|\eta_{b-jet}| < 2.5$, finding $(2.3 \pm 0.5)\%$, once again in agreement with the NLO prediction of $(1.8 \pm 0.4)\%$ (27).

The contrast between the theory vs. data comparisons in the $W + b$-jet and in the $Z + b$-jet final states is rather puzzling, and is one of the outstanding issues left open by the Tevatron data. From the theoretical perspective, the prediction of the $Z + b$-jet rate appears more challenging than the $W + b$-jet one, and thus more prone to a possible disagreement with data. $Z + b$-jet receives in fact at LO contributions from the reaction $bg \to Zb$, where the direct knowledge of the b-quark PDF is rather poor. One can replace this with the calculations of the $gg \to Zb\bar{b}$ process, recovering the PDF contribution from the integration over the phase-space for a collinear $g \to b\bar{b}$ emission in the initial state. But this, as mentioned above, leads to large logarithms, which then need to be resummed as one would do with the b-quark PDF, rendering the whole calculation more

complex.

A reassessment of the $W + b$-jet result, with a higher-luminosity update and an independent measurement by D0, is highly desirable. In particular, there is interest in the measurement of the E_T spectrum of the b-jet, and in a separate measurement of the associated production of two separate b-jets, to verify whether the discrepancy with NLO is limited to the theoretically more delicate single-jet case, or whether it appears also in the simpler two-jet case. Notice that the measurement of a W and a pair of b jets is also crucial for the understanding of the QCD backgrounds to the Higgs search in the channel $p\bar{p} \to WH$.

3.4 LHC: first findings

With the first 40pb^{-1} of data at $\sqrt{S} = 7$ TeV accumulated during 2010, the ATLAS and CMS experiments at the LHC have started an extremely rich programme of measurements, covering fields from the final-state structure of generic collisions, to searches for new particles. Of relevance to this review, the first measurements of V plus multijet production have already been published. Cross sections as a function of jet multiplicity, and transverse energy spectra for the leading and subleading jets, were measured by the ATLAS experiment (75). Jets were defined by the anti-k_T algorithm (5), with a radius parameter of $R = 0.4$, $E_T > 30$ GeV and $|\eta| < 2.8$, and the cross sections quoted for leptons satisfying the following kinematical constraints: $E_T^\ell > 20$ GeV, $|\eta_e| < 2.47$ (excluding $1.37 < |\eta_e| < 1.52$), $|\eta_e| < 2.4$, $p_T^\nu > 25$ GeV, $M_T > 40$ GeV and the ΔR separation between jet and leptons larger than 0.5. The results, and a comparison with both NLO and LO multiparton plus shower MC predictions, are shown in figs. 8 and 9. While the overall experimental uncertainty is still rather large, the

agreement of data and theory is good, both for the NLO parton-level predictions (taken, for up to two jets, from the MCFM code (17,18)) and for the multiparton plus shower MC calculations (ALPGEN (39) and SHERPA (11)). However a shower MC like PYTHIA, including the exact multiparton matrix elements only for the emission of the leading jet, describes the larger multiplicities much less accurately (7). Notice furthermore the behavior of the Berends scaling variable R_n, shown in the two lower plots of fig. 8. As anticipated in Table 2, for $E_T > 20$ GeV there is a large jump between R_1 and R_2, and a further decrease going to higher n values, confirming that the constant scaling is only very approximate.

Notice that the data vs. theory comparison shows slightly different features in the electron and muon final states, with a better agreement in the electron case. Since QCD does not distinguish between e and μ, both final states should ultimately lead to exactly the same assessment of the data vs. theory comparison. It is unlikely that the observed pattern can be caused by the minor selection differences between the electron and muon final states. The current differences should therefore be attributed to the still large experimental uncertainties, which will be greatly reduced as soon as higher-statistics samples will be collected and analyzed.

As mentioned in the introduction, associated production of jets and EW gauge bosons constitutes the leading SM background to searches for BSM particles. No signal for new physics has been found as yet, but these first searches (see for example (76–78), in the case of supersymmetry) have already extended the excluded regions well beyond what has been probed by the experiments at the Tevatron and at LEP. In the process, these analyses have validated the theoretical description of such final states, showing an excellent agreement between the data

and the sum of the several contributions from different SM multijet processes, as modeled by the calculations. An excellent example, from the ATLAS experiment (78), is given in fig. 10, which shows the spectrum of missing transverse energy E_T^{miss} in final states with a lepton (e or μ) with $p_T > 20$ GeV and at least three jets with $E_T > 30$ GeV, of which at least one is above 60 GeV. The data receive SM contributions from processes like inclusive multijet production (where the missing energy arises from the detector resolution), W and Z plus jets and top quark production. The agreement between the predictions and the data is excellent, providing good confidence that the basic backgrounds to the searches of supersymmetry are properly understood.

4 CONCLUSIONS AND OUTLOOK

The understanding of V+jets is essential to the search for, and measurement of, new heavy particles. But it also provides a rich domain for studies of perturbative QCD, as it explores a great variety of kinematical and dynamical configurations. This is the first case in hadron collisions where NLO calculations for multiparton final states are available. Their comparison with data allows a first phenomenological evaluation of such complex calculations. This will test, for example, the choice of the several possible functional forms for the renormalization scale, an open issue which is critical for the reliable determination of the NLO scale uncertainty. These studies are starting only now, and will require measurements mapping the multijet kinematical correlations. Of particular interest will be kinematical configurations with several different scales. Production of many low-E_T jets can be seen as a mere radiative correction to the primary hard process of V production, at the scale M_V. This is reflected in the Berends scaling of mul-

tijet rates. Production of jets with $E_T > M_V$, on the other hand, introduces a new hard scale, whose interplay with M_V is reflected in the large variation of the NLO cross sections as the renormalization scale is changed between M_W and $H_T = \sum_{jets} E_T$. Further complexity will arise in the presence of jets with $E_T \gg M_V$ together with jets having $E_T \ll M_V$; these final states could be of interest for several searches of new particles. Here, again, potentially large Sudakov effects can challenge the reliability of NLO calculations, possibly requiring the resummation of large logarithms and a mixed NLO plus shower approach. The large cross sections available at the LHC, and the much greater range of jet energies accessible there, will provide a fertile terrain for unprecedented studies of the perturbative QCD dynamics, which we are only now starting to explore.

Literature Cited

1. M. L. Mangano, Eur. Phys. J. C **59**, 373 (2009).
2. J. M. Campbell, J. W. Huston and W. J. Stirling, Rept. Prog. Phys. **70**, 89 (2007).
3. Mangano M.L. and Stelzer T.J., Ann. Rev. Nucl. Part. Sci. **55**, 555 (2005).
4. S. Alekhin *et al.*, arXiv:1101.0536 [hep-ph].
5. Salam G.P., Eur. Phys. J. C **67**, 637 (2010).
6. A. Buckley *et al.*, arXiv:1101.2599 [hep-ph].
7. T. Sjostrand, S. Mrenna and P. Z. Skands, JHEP **0605**, 026 (2006).
8. T. Sjostrand, S. Mrenna and P. Z. Skands, Comput. Phys. Commun. **178**, 852 (2008).
9. G. Corcella *et al.*, arXiv:hep-ph/0210213.
10. M. Bahr *et al.*, Eur. Phys. J. C **58**, 639 (2008).

11. T. Gleisberg et al, JHEP **0902**, 007 (2009).
12. F. A. Berends, H. Kuijf, B. Tausk and W. T. Giele, Nucl. Phys. B **357**, 32 (1991).
13. R. K. Ellis, G. Martinelli and R. Petronzio, Nucl. Phys. B **211**, 106 (1983).
14. P. B. Arnold and M. H. Reno, Nucl. Phys. B **319**, 37 (1989) [Erratum-ibid. B **330**, 284 (1989)].
15. P. Arnold, R. K. Ellis and M. H. Reno, Phys. Rev. D **40**, 912 (1989).
16. W. T. Giele, E. W. Glover and D. A. Kosower, Nucl. Phys. B **403**, 633 (1993).
17. J. M. Campbell and R. K. Ellis, Phys. Rev. D **65**, 113007 (2002).
18. J. M. Campbell, R. K. Ellis and D. L. Rainwater, Phys. Rev. D **68**, 094021 (2003).
19. R. K. Ellis, K. Melnikov, G. Zanderighi, JHEP **0904**, 077 (2009).
20. C. F. Berger, Z. Bern, L. J. Dixon *et al.*, Phys. Rev. Lett. **102**, 222001 (2009).
21. R. K. Ellis, K. Melnikov, G. Zanderighi, Phys. Rev. **D80**, 094002 (2009).
22. C. F. Berger, Z. Bern, L. J. Dixon *et al.*, Phys. Rev. **D80**, 074036 (2009).
23. C. F. Berger, Z. Bern, L. J. Dixon *et al.*, Phys. Rev. **D82**, 074002 (2010).
24. C. F. Berger, Z. Bern, L. J. Dixon *et al.*, arXiv:1009.2338 [hep-ph].
25. W. T. Giele, S. Keller and E. Laenen, Nucl. Phys. Proc. Suppl. **51C**, 255 (1996).
26. W. T. Giele, S. Keller and E. Laenen, Phys. Lett. B **372**, 141 (1996).
27. J. M. Campbell, R. K. Ellis, F. Maltoni and S. Willenbrock, Phys. Rev. D **69**, 074021 (2004).
28. F. Febres Cordero, L. Reina and D. Wackeroth, Phys. Rev. D **74**, 034007

(2006).

29. F. Febres Cordero, L. Reina and D. Wackeroth, Phys. Rev. D **80**, 034015 (2009).
30. F. F. Cordero, L. Reina and D. Wackeroth, PoS **RADCOR2009**, 055 (2010).
31. S. Badger, J. M. Campbell and R. K. Ellis, JHEP **1103**, 027 (2011).
32. V. Hirschi, R. Frederix, S. Frixione, M. V. Garzelli, F. Maltoni and R. Pittau, arXiv:1103.0621 [hep-ph].
33. S. Alioli, P. Nason, C. Oleari and E. Re, JHEP **1101**, 095 (2011).
34. S. Catani, F. Krauss, R. Kuhn and B. R. Webber, JHEP **0111**, 063 (2001).
35. F. Krauss, JHEP **0208**, 015 (2002).
36. L. Lonnblad, JHEP **0205**, 046 (2002).
37. M. L. Mangano, M. Moretti, F. Piccinini and M. Treccani, JHEP **0701**, 013 (2007).
38. S. Mrenna and P. Richardson, JHEP **0405**, 040 (2004).
39. M. L. Mangano et al, JHEP **0307**, 001 (2003).
40. F. Maltoni and T. Stelzer, JHEP **0302**, 027 (2003).
41. C. G. Papadopoulos and M. Worek, Eur. Phys. J. C **50**, 843 (2007).
42. L. Lonnblad, Comput. Phys. Commun. **71**, 15 (1992).
43. J. Alwall *et al.*, Eur. Phys. J. C **53**, 473 (2008).
44. F. Krauss, A. Schalicke, S. Schumann and G. Soff, Phys. Rev. D **70**, 114009 (2004).
45. F. Krauss, A. Schalicke, S. Schumann and G. Soff, Phys. Rev. D **72**, 054017 (2005).
46. S. Frixione and B. R. Webber, JHEP **0206**, 029 (2002).

47. S. Frixione and B. R. Webber, arXiv:hep-ph/0207182.
48. P. Nason, JHEP **0411**, 040 (2004).
49. S. Frixione, P. Nason and C. Oleari, JHEP **0711**, 070 (2007).
50. K. Hamilton and P. Nason, JHEP **1006**, 039 (2010).
51. S. Hoche, F. Krauss, M. Schonherr and F. Siegert, arXiv:1009.1127 [hep-ph].
52. D. Acosta *et al.* [CDF Coll.], Phys. Rev. Lett. **94**, 091803 (2005).
53. A. Abulencia *et al.* [CDF Coll.], J. Phys. G **34**, 2457 (2007).
54. V. M. Abazov *et al.* [D0 Coll.], Phys. Rev. Lett. **100**, 102002 (2008).
55. V. M. Abazov *et al.* [D0 Coll.], arXiv:1010.0262 [hep-ex].
56. G. Aad *et al.* [Atlas Coll.], JHEP **1012**, 060 (2010).
57. V. Khachatryan *et al.* [CMS Coll.], JHEP **1101**, 080 (2011).
58. S. D. Ellis, R. Kleiss and W. J. Stirling, Phys. Lett. B **154**, 435 (1985).
59. H. L. Lai *et al.* [CTEQ Coll.], Eur. Phys. J. C **12** (2000) 375.
60. T. Aaltonen *et al.* [CDF Coll.], Phys. Rev. **D77**, 011108 (2008).
61. T. Aaltonen *et al.* [CDF Coll.], Phys. Rev. Lett. **100**, 102001 (2008).
62. V. M. Abazov *et al.* [D0 Coll.], Phys. Lett. **B669**, 278-286 (2008).
63. V. M. Abazov *et al.* [D0 Coll.], Phys. Lett. **B678**, 45-54 (2009).
64. G. C. Blazey *et al.*, in Proceedings of the Workshop: QCD and Weak Boson Physics in Run II, edited by U. Baur, R. K. Ellis, and D. Zeppenfeld, arXiv:hep-ex/0005012.
65. O. Salto Bauza, FERMILAB-THESIS-2008-17.
66. V. M. Abazov *et al.* [D0 Coll.], Phys. Lett. **B682**, 370-380 (2010).
67. V. M. Abazov *et al.* [D0 Coll.], Phys. Rev. Lett. **102**, 192002 (2009).
68. T. Aaltonen *et al.* [CDF Coll.], Phys. Rev. **D81**, 052006 (2010).
69. U. Baur *et al.*, Phys. Lett. B **318**, 544 (1993).

70. T. Aaltonen *et al.* [CDF Coll.], Phys. Rev. Lett. **100**, 091803 (2008).

71. V. M. Abazov *et al.* [D0 Coll.], Phys. Lett. **B666**, 23-30 (2008).

72. T. Aaltonen *et al.* [CDF Coll.], Phys. Rev. Lett. **104**, 131801 (2010).

73. T. Aaltonen *et al.* [CDF Coll.], Phys. Rev. **D79**, 052008 (2009).

74. V. M. Abazov *et al.* [D0 Coll.], Phys. Rev. Lett. **94**, 161801 (2005).

75. G. Aad *et al.* [ATLAS Coll.], arXiv:1012.5382 [hep-ex].

76. V. Khachatryan *et al.* [CMS Coll.], arXiv:1101.1628 [hep-ex].

77. G.Aad *et al.* [Atlas Coll.], arXiv:1102.5290 [hep-ex].

78. J. B. G. da Costa *et al.* [Atlas Coll.], arXiv:1102.2357 [hep-ex].

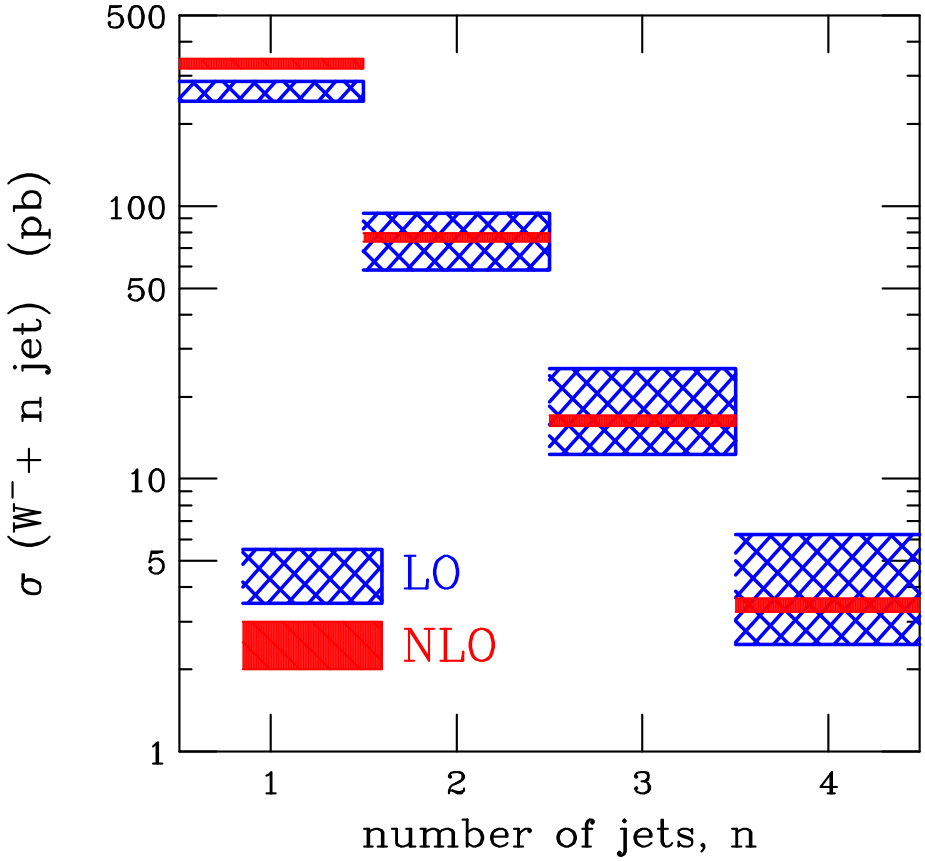

Figure 1: Summary of LO and NLO cross sections for W^-+ jet production at the 7 TeV LHC, adapted from Table I of Ref. (24). The LO scale uncertainty is given by the hashed (blue) region, the NLO uncertainty by the shaded (red) one.

Table 1: Parton-level LO cross section ratios $R_n = \sigma_{W+n}/\sigma_{W+(n-1)}$ at the Tevatron, as a function of parton E_T threshold, for partons with $|\eta| < 2.5$ and $\Delta R > 0.7$.

Jet E_T cut	R_1	R_2	R_3	R_4
$E_T > 10$ GeV	0.25	0.24	0.22	0.20
$E_T > 20$ GeV	0.11	0.16	0.14	0.12
$E_T > 30$ GeV	0.05	0.12	0.10	0.08
$E_T > 50$ GeV	0.02	0.09	0.05	0.04

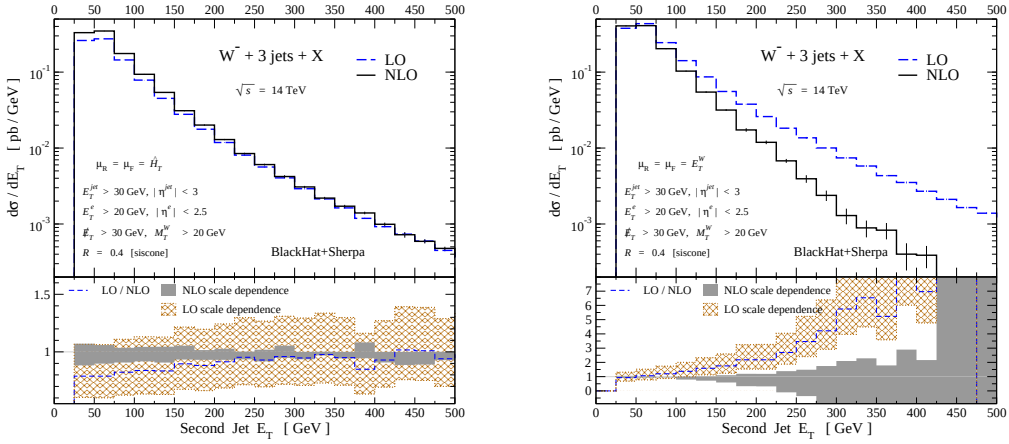

Figure 2: A comparison of the LO and NLO predictions for the second jet E_T in $W^- + 3$ jet events at the LHC using the two scale choices $\mu = \hat{H}_T$ (left) and $\mu = E_T^W$ (right). The figures are taken from Ref. (22).

Table 2: Same as previous Table, for the LHC (7 TeV).

Jet E_T cut	R_1	R_2	R_3	R_4
$E_T > 10$ GeV	0.35	0.37	0.33	0.29
$E_T > 20$ GeV	0.17	0.27	0.24	0.21
$E_T > 30$ GeV	0.10	0.23	0.19	0.17
$E_T > 50$ GeV	0.08	0.21	0.13	0.12

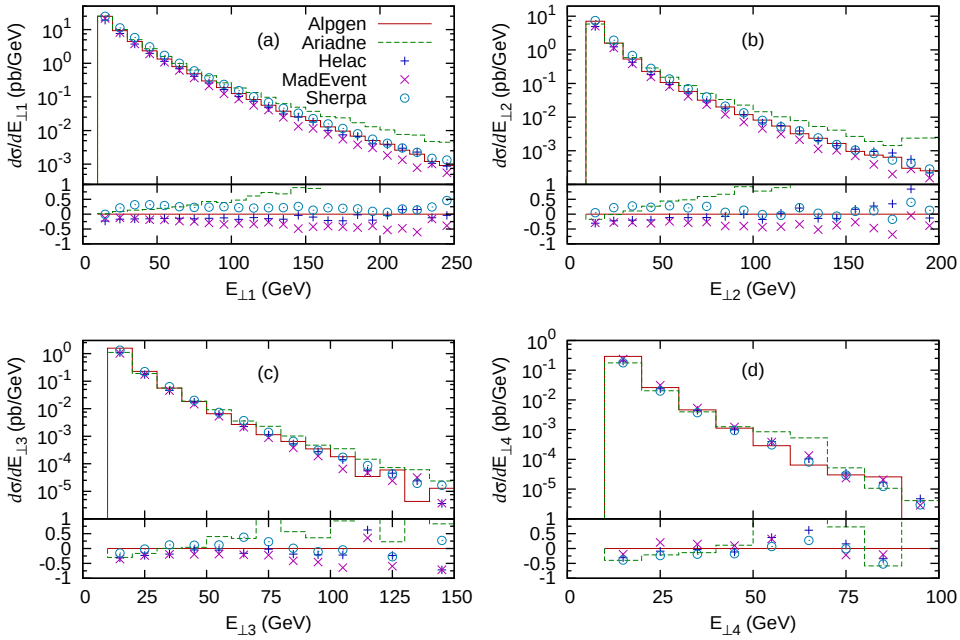

Figure 3: Comparison among the predictions of different matching schemes for W+jets (43): E_T spectra of the four-leading jets at the Tevatron in inclusive $W + X$ final states at the Tevatron. The relative differences among the various calculations and the reference Alpgen predictions are shown in the lower insets of each plot.

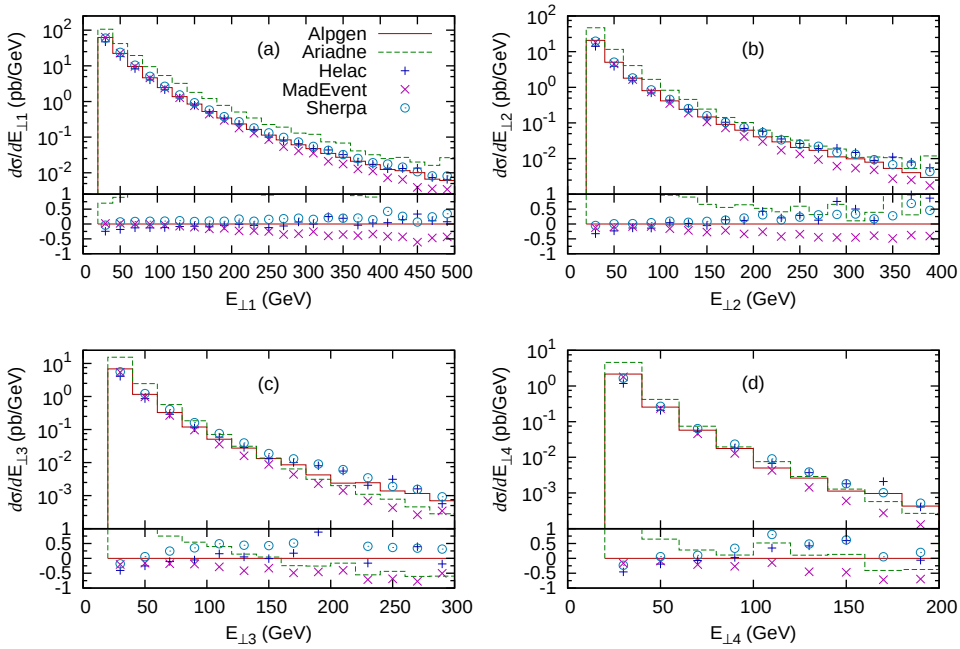

Figure 4: Same as Fig. 4, for the LHC ($\sqrt{S} = 14$ TeV).

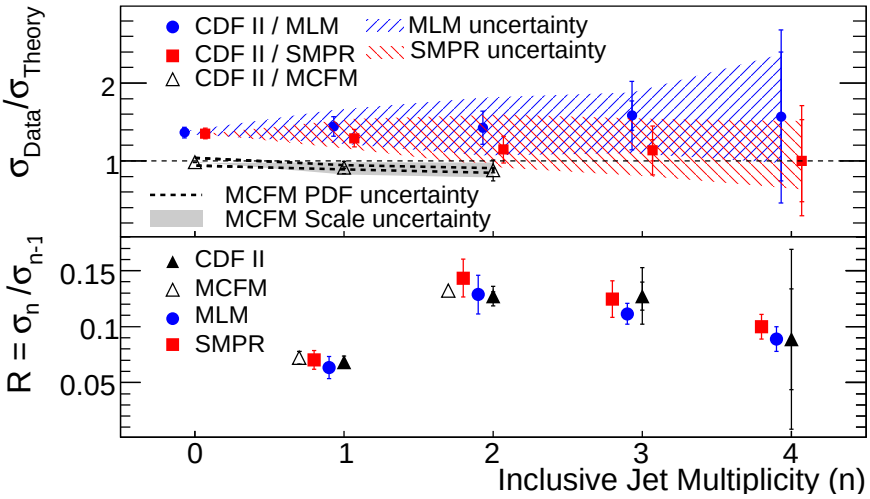

Figure 5: W+multijet cross section measurements (60) from the Tevatron experiment CDF. Jet selection cuts and the displayed theoretical predictions are listed in the main text.

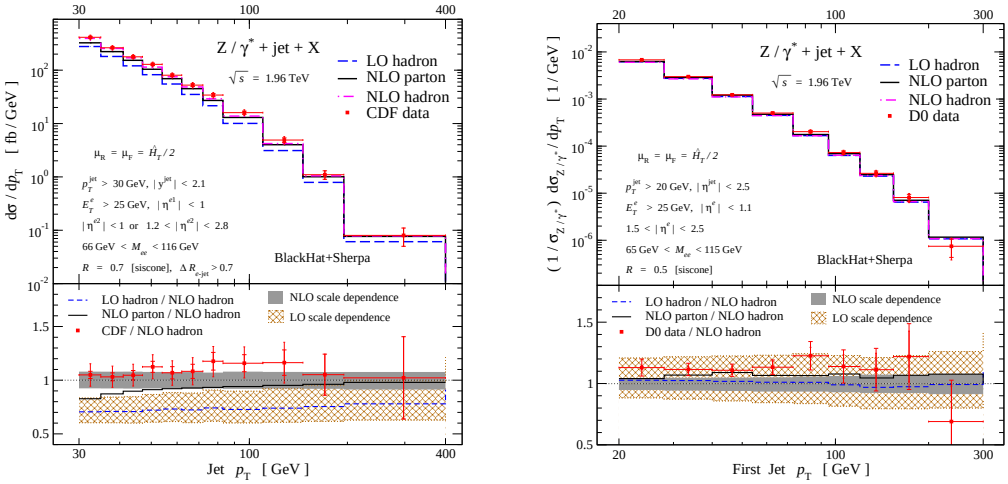

Figure 6: CDF inclusive jet spectrum (left) and D0 leading-jet spectrum (right), in Z+jets events. The curves are taken from ref. (23), where the NLO calculations were presented.

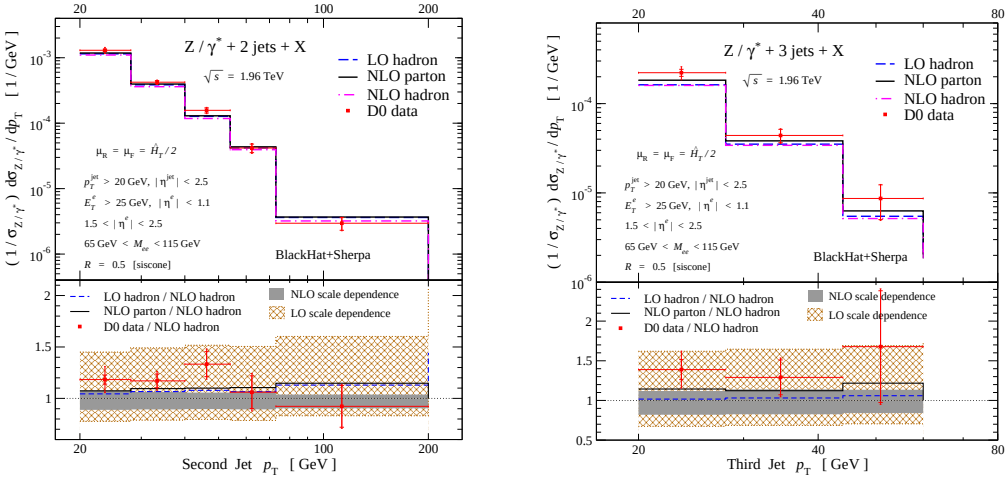

Figure 7: Spectra of the second and third jet in Z+jets events. The curves are taken from ref. (23), where the NLO calculations were presented.

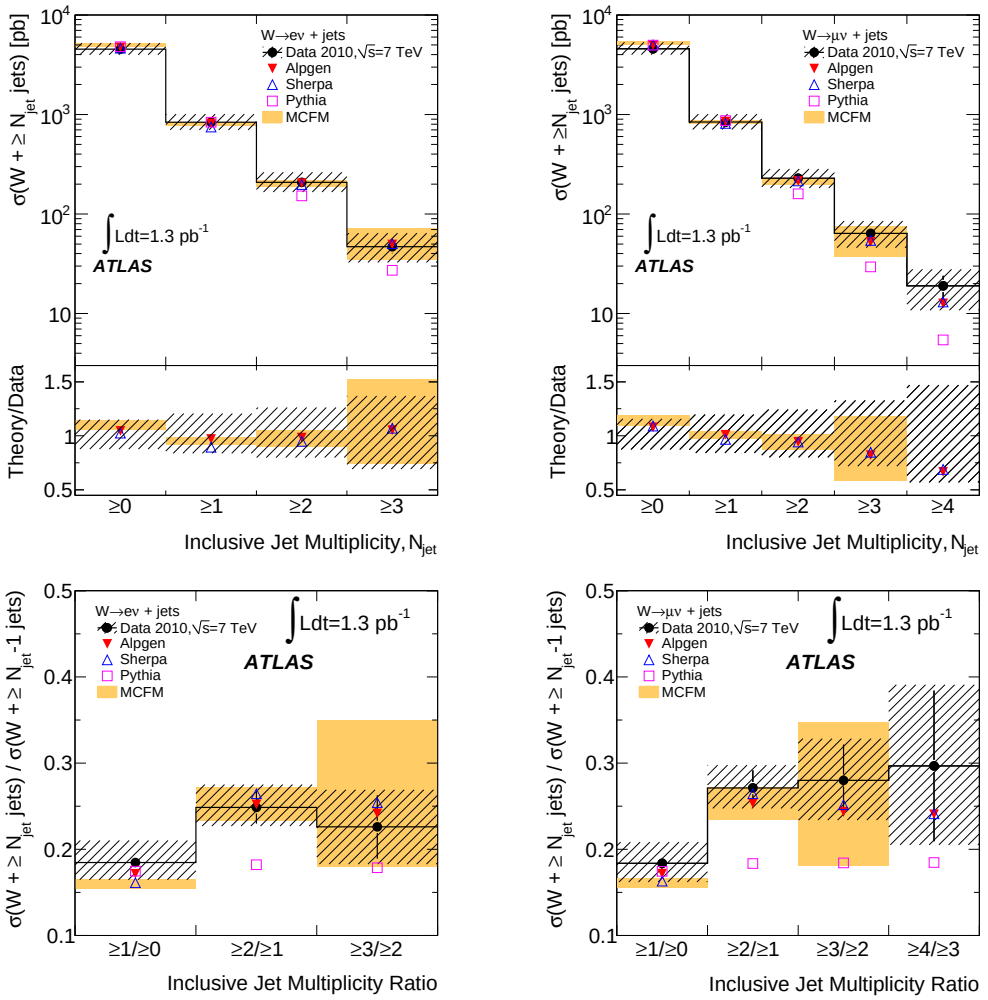

Figure 8: Multijet cross sections in W+jet events at the LHC (upper plots) and cross section ratios (lower plots), measured by the ATLAS experiment (75) in the $W \to e\nu_e$ (left) and $W \to \mu\nu_\mu$ (right) final states, compared with various theoretical predictions. The hashed areas represent the total experimental uncertainty, the shaded ones show the theoretical uncertainty (at NLO for up to two jets, at LO beyond) from the MCFM MC (17).

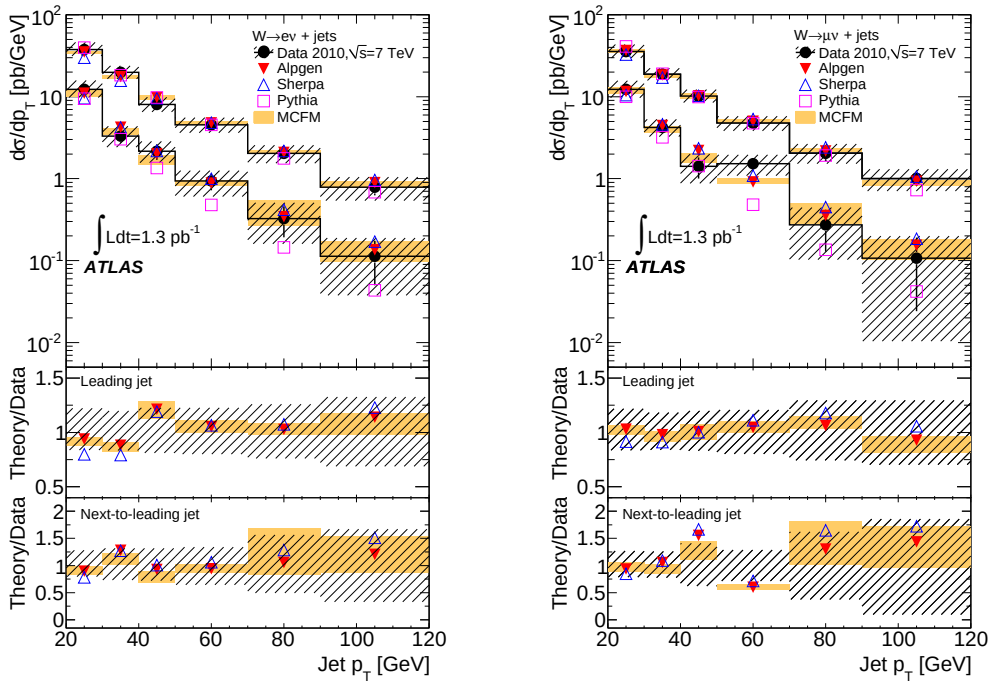

Figure 9: Transverse energy spectra of the leading and next-to-leading jets in W+jet events, measured by the ATLAS experiment (75) in the $W \to e\nu_e$ (left) and $W \to \mu\nu_\mu$ (right) final states, compared with various theoretical predictions.

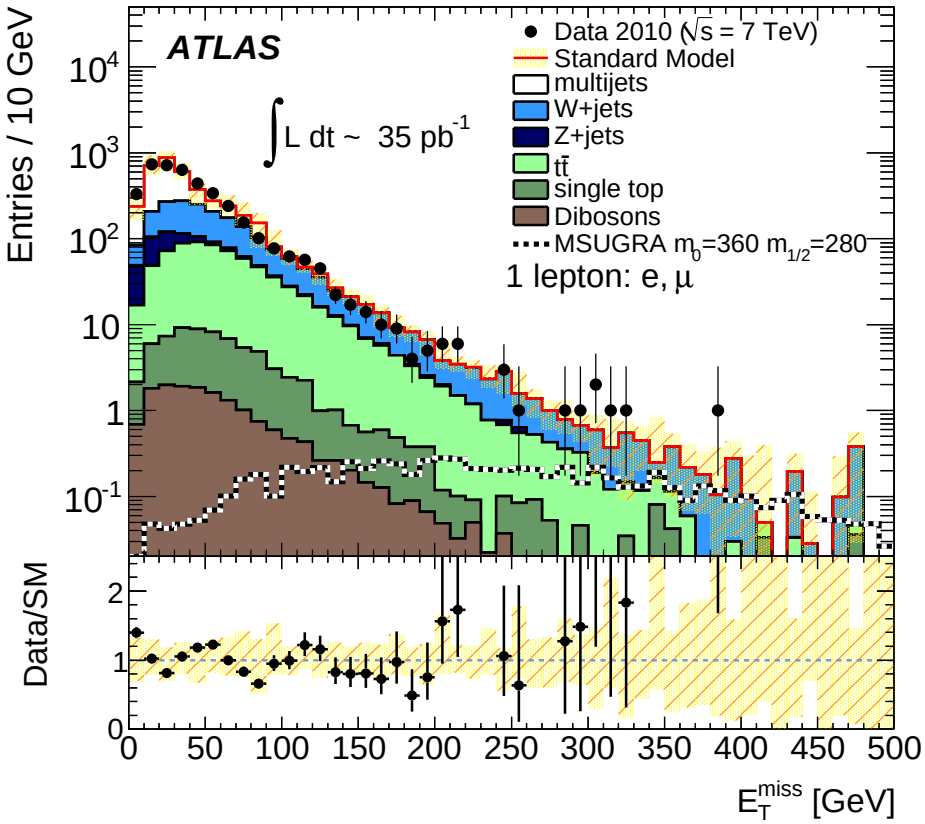

Figure 10: The spectrum of missing transverse energy in events with leptons and jets observed (78) by the ATLAS experiment at the LHC, compared to the predictions of the Standard Model.